# Superconductivity in WP single crystals

Ziyi Liu,[1,2] Wei Wu,[1,3,4,*] Zhenzheng Zhao,[1] Hengcan Zhao,[1,4] Jian Cui,[1] Pengfei Shan,[1] Jiahao Zhang,[1,4] Changli Yang,[1,5] Peijie Sun,[2] Yuan Wei,[1,4] Shiliang Li,[1,3] Jinggeng Zhao,[2] Yu Sui,[2] Jinguang Cheng,[1,3] Li Lu,[1,5,3] Jianlin Luo,[1,5,3,†] and Guangtong Liu[1,3,‡]

[1]*Beijing National Laboratory for Condensed Matter Physics, Institute of Physics, Chinese Academy of Sciences, Beijing 100190, China*

[2]*Department of Physics, Harbin Institute of Technology, Harbin, Heilongjiang 150001, China*

[3]*Songshan Lake Materials Laboratory, Dongguan, Guangdong 523808, China*

[4]*University of Chinese Academy of Sciences, Beijing 100049, China*

[5]*Collaborative Innovation Center of Quantum Matter, Beijing 100871, China*

(Received 22 January 2019; revised manuscript received 8 April 2019; published 21 May 2019)

We report the discovery of superconductivity in high-quality single crystals of transition-metal pnictides WP grown by chemical vapor transport method. Bulk superconductivity is observed at $T_c \sim 0.8$ K at ambient pressure by electrical resistivity, ac magnetic susceptibility, and specific-heat measurements. The effects of magnetic field on the superconducting transitions are studied, leading to a large anisotropy parameter around 2 with the in-plane and out-of-plane upper critical fields of $\mu_0 H_{c2,\parallel} = 17.2$ mT and $\mu_0 H_{c2,\perp} = 8.5$ mT, respectively. The low value of electron-phonon coupling estimated from the normal-state resistivity and specific-heat measurements suggest that WP is a weak-coupling BCS superconductor. Our finding demonstrates that WP is the first superconductor among 5*d*–transition metal pnictides with MnP-type structure at ambient pressure, which will help in the search for new superconductors in transition-metal pnictides.

DOI: 10.1103/PhysRevB.99.184509

## I. INTRODUCTION

The novel and intriguing behaviors in transition metal pnictides have long attracted the attention of researchers due to multiple quantum orders and competing phenomena. One of the examples is the recently discovered pressure-induced superconductivity in CrAs and MnP [1–4]. At ambient conditions, both CrAs and MnP adopt the MnP-type (B31) structure, belonging to the large family of transition metal pnictides with a general formula $MX$ ($M$ = transition metal, $X$ = P, As, Sb). Most of the $MX$ compounds crystallize in either the hexagonal NiAs-type structure or the orthorhombic MnP-type structure, for which the latter is a distorted structure of the former with small shifts of atomic positions [5].

By analyzing the structures of these phosphides as a function of the electron number per formula unit, Tremel *et al.* [6] found that the MnP-type phases can only exist in the transition metal phosphide compounds with the number of valence electrons ranging from 11 to 14, such as CrP, MnP, FeP, CoP, RuP, WP, and IrP. Among these phosphides, MnP and FeP are metals with a unique magnetic structure consisting of a helical arrangement of spins with net antiferromagnetic ordering [7,8]. CrP and CoP are normal metals with Fermi-liquid ground states [9,10]. RuP is a metal of 4*d*–transitional metal phosphides with charge-density wave (CDW) order [11]. Compared to that of 3*d*–transitional metal phosphides, the relatively wide energy band and the extended wave function in 5*d*–transition metal pnictides, such as WP and IrP, lead to a smaller density of states (DOS) and more overlap of 5*d* orbital. Therefore, the electrons are itinerant and no magnetic ordering was observed in 5*d*–transition metal pnictides [12].

To date, superconductivity is found only in pressurized-MnP and Rh-doped RuP among phosphide compounds [11]. Moreover, the similarity of the superconducting phase diagrams between CrAs/MnP and Fe/Cu-based superconductors points to possible unconventional superconductivity [13,14]. Therefore, it is of high interest to explore whether intrinsic superconductivity at ambient pressure can be achieved in the MnP family.

Here we report superconductivity in high-quality WP single crystals at ambient pressure as an example in the MnP family. The electrical resistivity, ac magnetic susceptibility, and specific-heat measurements revealed a bulk superconductivity with $T_c \sim 0.8$ K. The magnetotransport measurements showed that upper critical fields have an anisotropy parameter of around 2. The low value of electron-phonon coupling estimated from the normal-state resistivity and specific-heat measurements suggest that WP is a weak coupling BCS superconductor.

## II. EXPERIMENTAL DETAILS

The polycrystalline samples were prepared using a conventional solid-state reaction method. Stoichiometric amounts of W and P powders were mixed thoroughly and pressed into pellets. The pellets were then sealed in an evacuated quartz tube. Considering the fact that red phosphorus sublimates at about ~416 °C and tungsten reacts with oxygen, sulfur, and

*welyman@iphy.ac.cn
†jlluo@iphy.ac.cn
‡gtliu@iphy.ac.cn

 

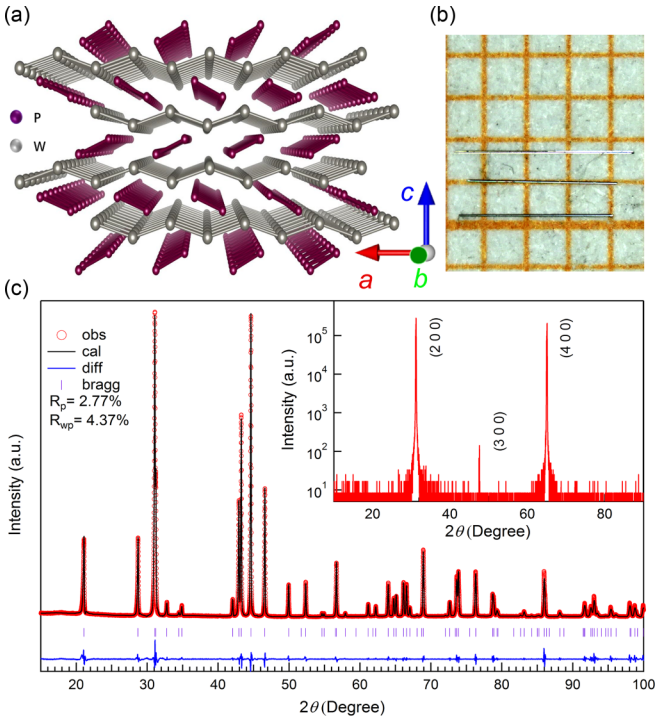


FIG. 1. Structural characterization of WP. (a) Crystal structure of WP. (b) An optical image of the as-grown WP single crystals on a 1 mm × 1 mm grid. (c) Room-temperature x-ray diffraction (XRD) spectra and the Rietveld refinement of polycrystalline WP. The open circle, solid line, and lower solid line represent experimental, calculated, and difference XRD patterns, respectively. The inset shows the XRD pattern for WP single crystals.

nitrogen higher than 400 °C, the sealed ampoule was heated to 400 °C over 10 h and kept for 20 h, then heated to 1000 °C over 40 h and kept for about 3 days at this temperature before cooling down to room temperature. WP crystallizes in an orthorhombic structure with space group *Pnma* (no. 62), as illustrated in Fig. 1(a). The crystal structure of the compound was verified by Rietveld refinement [15] of a powder x-ray diffraction (XRD) pattern collected on polycrystalline WP at ambient conditions. As shown in Fig. 1(c), all the diffraction peaks can be well indexed to the orthorhombic phase WP (space group *Pnma*) with lattice parameters $a = 5.7222(6)$ Å, $b = 3.2434(9)$ Å, and $c = 6.2110(6)$ Å, which are in good agreement with previously reported values [16–18].

Due to the high melting point of WP, it is very difficult to grow WP single crystals using conventional melting technique, such as the Bridgman method. For the growth of WP single crystals, we employed the chemical vapor transport (CVT) method which has been successfully used to grow pnictides such as CrP, MoP, NbP, and TaP [19–21]. The well-mixed starting materials of iodine (0.1 g) and WP polycrystalline powders (0.5 g) were placed at one end of a quartz tube with a diameter of 2 cm and a length of 20 cm. Then the tube was sealed under high vacuum and placed in a two-zone furnace with a temperature gradient from 1100 °C (source end) to 1050 °C (sink end) for one week followed by slowly heating the sink end to 1150 °C over a 1-month period. This process is the key to obtain WP single crystals and we call it a "sink-source reverse" method. After this process, the furnace was naturally cooled to room temperature by turning off the power. Finally, shiny needlelike single crystals were found at the source end. By this method, we successfully synthesized the large single crystals of WP with a typical dimension of $0.1 \times 0.1 \times 4.0$ mm$^3$ as shown in Fig. 1(b). The *b*-axis direction relative to the crystal morphology was determined from a single crystal lying on a beveled silicon slice on a powder diffractometer. The XRD pattern in the inset of Fig. 1(c) shows only ($l$00) peaks with no impurities, indicating the high quality of WP single crystals and the *b* axis is parallel to the needle-shaped sample. The chemical compositions of the single crystals were determined by a scanning electron microscope (SEM) with an energy dispersive x-ray spectrometer (EDS). The atomic ratio between W and P is found to be 49.49 : 50.51, indicating that the as-prepared single crystals have the composition W : P = 1 : 1.

The electrical resistivity was measured with the conventional four-probe method using a Quantum Design physical property measurement system (PPMS) from 300 to 2 K. For temperatures below 2 K, the experiments were performed on a top-loading He3 refrigerator with a superconducting magnet up to 15 T. ac magnetic susceptibility was measured by a mutual inductance coil. The sample and a similar volume piece of lead (Pb) were put into the coil and fixed by glue. The diamagnetic signal due to the superconductivity transition was estimated by comparing with the diamagnetic signal of Pb. An excitation current of 0.5 mA with a frequency of 1117 Hz was applied to the primary coil and output signal across two oppositely wound secondary coils was picked up with a Standford Research SR830 lock-in amplifier.

## III. RESULTS AND DISCUSSIONS

Figure 2(a) shows the temperature dependence of electrical resistivity measured on three typical WP single crystals (S1, S2, and S3) between 300 and 0.3 K in zero field. The WP has a normal-state resistivity ∼40 $\mu\Omega$ cm at room temperature with a residual resistivity ratio (RRR) defined as $R$(300 K)/$R$(1.5 K) of ∼37. A linear dependence of resistivity $\rho(T)$ on temperature has been observed in the temperature range from 300 to 60 K. Then $\rho(T)$ further decreases to a temperature-independent constant as the temperature reduced to 1.5 K, indicating that WP has a metallic conduction property. As the sample is further cooled, $\rho(T)$ drops steeply at about 0.85 K, signaling the onset of superconductivity. From the upper left inset of Fig. 2(a), it can be seen that the superconducting transitions for these three samples are very sharp. Especially for sample S3, the transition width is less than 20 mK, indicative of the high quality of the sample. It should be noted that the different transition behaviors of these three samples are probably due to the different sample qualities [22,23]. If we define the superconducting transition temperature $T_c$ as the temperature at the midpoint of the resistive transition, it is found that $T_c$ for these samples are very close, ranging from 0.834 and 0.840 K, further demonstrating the samples are uniform and of high quality.

The superconducting transition in WP single crystals is further characterized by the low-temperature ac susceptibility measurement. Figure 2(b) shows the magnetic field

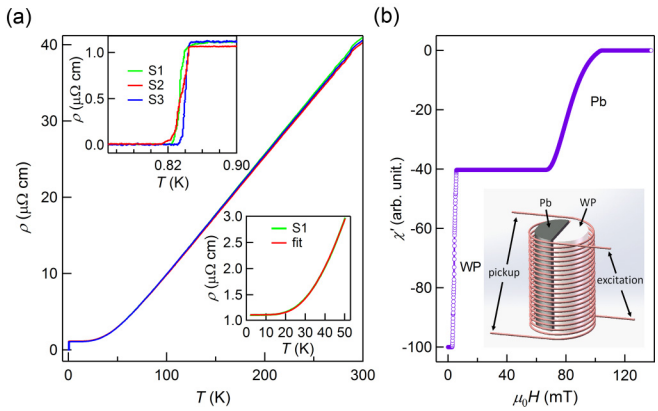


FIG. 2. Superconductivity characterization in WP single crystals. (a) Temperature-dependent resistivity $\rho(T)$ for three typical WP single crystals (S1, S2, and S3) between 300 and 0.3 K in zero external magnetic field. The upper left inset is an enlarged view of superconducting transitions at low temperatures. The lower right inset shows the comparison between the experimental data and the fitting result with the Bloch-Gruneisen function. (b) ac magnetic susceptibility for WP single crystals measured at 0.3 K. The inset is a schematic diagram of the ac magnetic susceptibility measurement setup.

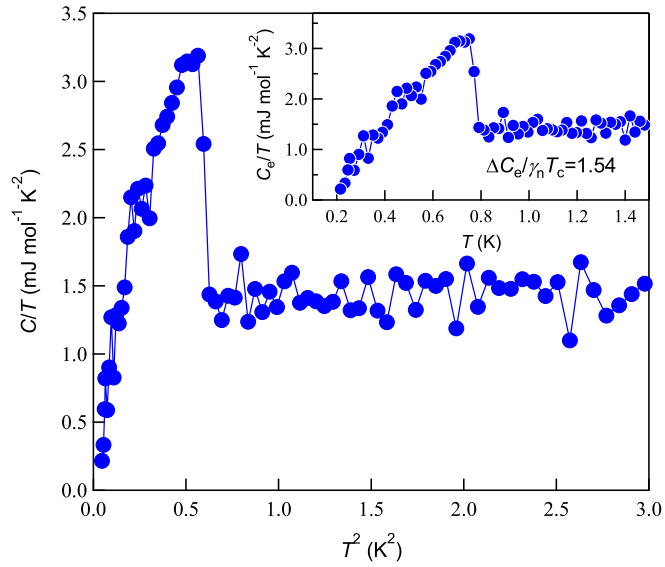


FIG. 3. Low-temperature specific heat of WP single crystals plotted as $C/T$ vs $T^2$ at zero field. The inset shows temperature dependence of normalized electronic specific heat $C_e/T$.

dependence of ac susceptibility $\chi'$ at 0.3 K. As the external magnetic field $H$ decreases to 0.1 T, a broad diamagnetic signal corresponding to the superconductivity of Pb is observed. Then when the magnetic field approaches $H = 11$ mT, another large diamagnetic signal was detected, which is ascribed to the superconductivity of WP. Moreover, the field is in good agreement with the upper critical field measurement which will be shown in the following section. Compared to Pb, the signal of $\chi'$ from WP is much stronger and sharper, further demonstrating the high quality of the WP single crystals.

To further elucidate the bulk superconductivity in WP single crystals, we have carried out the specific-heat measurement with the dilution refrigerator down to 0.2 K. The result is shown in Fig. 3. A clear specific-heat jump can be observed at $T_c \sim 0.8$ K, demonstrating that bulk superconductivity is achieved. Moreover, the $T_c$ observed in the specific-heat data is very consistent with that determined from the electrical resistivity measurement.

To explore the superconducting phase diagram of WP single crystals, the temperature-dependent resistance $R(T)$ is systematically measured under different external applied magnetic fields. The inset of Fig. 4(a) shows the corresponding results for sample S3 under the magnetic field from 0 to 12.5 mT. As the magnetic field increases, the superconducting transition temperature $T_c$ shifts to lower temperature and the superconductivity is completely suppressed at $\mu_0 H = 12.5$ mT. Figure 4(a) summarizes the upper critical field $\mu_0 H_{c2}$ as a function of temperature $T_c$, where $T_c$ is defined as the temperature at the midpoint of the resistive transition. A linear temperature dependence is observed for $\mu_0 H_{c2}$, which can be well fitted by the Werthamer-Helfand-Hohenberg (WHH) equation given by

$$\mu_0 H_{c2}(0) = A T_c \frac{d\mu_0 H_{c2}}{dT}|_{T=T_c}, \quad (1)$$

where $A$ is $-0.693$. As shown by the dashed lines, the best fittings yield $\mu_0 H_{c2}(0) = 11.8$, 9.0, and 12.5 mT for samples S1, S2, and S3, respectively. A similar observation has been made in MnP [4]. The obtained $\mu_0 H_{c2}(0)$ allows us to estimate the Ginzburg-Landau coherence length $\xi = 1642$ Å according to the relationship $\mu_0 H_{c2}(0) = \Phi_0/2\pi\xi^2$, where $\Phi_0 = 2.067 \times 10^{-15}$ Wb is the magnetic-flux quantum.

The anisotropic upper critical field of WP single crystals is confirmed by the experiments with tilted magnetic field. The upper left inset of Fig. 4(b) shows the angular dependent $R(H)$ at 0.3 K, where $\theta$ is the tilt angle between the normal of the sample plane and the direction of the applied magnetic field [right lower inset of Fig. 4(b)]. The superconducting transition shifts to higher field with the external magnetic field rotating from the perpendicular ($\theta = 0°$) to parallel ($\theta = 90°$) direction. Figure 4(b) plots the upper critical field $\mu_0 H_{c2}$ extracted from the inset of Fig. 4(b) as a function of the tilted angle $\theta$. Clearly, the out-of-plane upper critical field $\mu_0 H_{c2,\perp}$ is much smaller than the in-plane upper critical field $\mu_0 H_{c2,\parallel}$, demonstrating strong anisotropic transport properties in WP single crystals.

To access the superconducting mechanism of WP, we first performed fitting the normal state resistivity with the Bloch-Gruneisen function [24],

$$\rho(T) = \rho(0) + A\left(\frac{T}{\Theta_D}\right)^5 \int_0^{\Theta_D/T} \frac{x^5}{(e^x - 1)(1 - e^{-x})}\, dx, \quad (2)$$

where $A$ is a constant and $\Theta_D$ is an effective Debye temperature. From the lower right inset of Fig. 2(a), one can see that the experimental data can be well described by the Bloch-Gruneisen function. The best fit gives the Debye temperature $\Theta_D = 238$ K, from which the electron-phonon coupling strength $\lambda_{ep}$ can be estimated from the McMillan

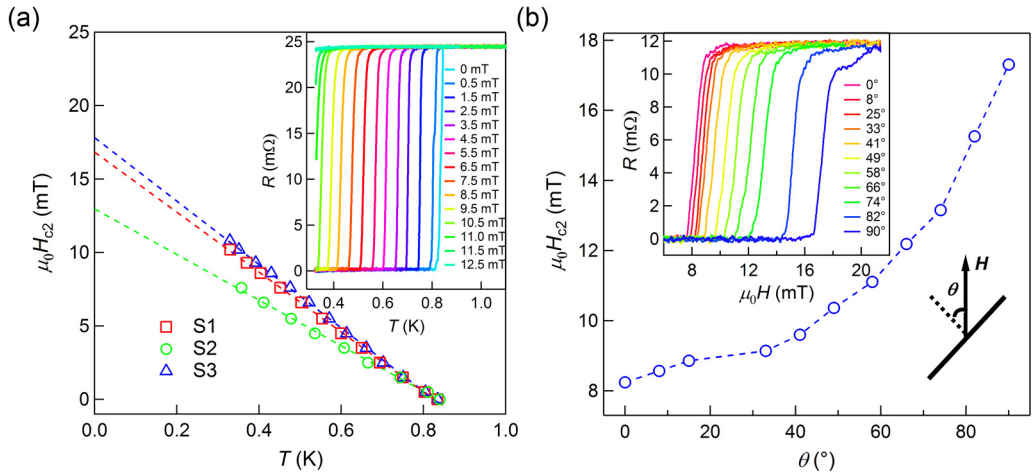


FIG. 4. (a) Upper critical field $H_{c2}$ vs temperature phase diagram of WP single crystals. The dashed lines denote the Werthamer-Helfand-Hohenberg (WHH) fits to sample S1, S2, and S3, respectively. Inset: Temperature dependence of the resistance of sample S3 in different perpendicular magnetic fields. (b) Angular dependence of the upper critical field $\mu_0 H_{c2}$ for sample S1. The left upper inset shows the magnetic field dependence of the resistance for sample S1 measured at $T = 0.3$ K with different tilt angle $\theta$. The right lower inset shows the scheme of our tilt experimental setup.

formula [25],

$$\lambda_{ep} = \frac{1.04 + \mu^* \mathrm{In}\left(\frac{\Theta_D}{1.45T_c}\right)}{(1 - 0.62\mu^*)\mathrm{In}\left(\frac{\Theta_D}{1.45T_c}\right) - 1.04}, \quad (3)$$

where $\mu^*$ is the repulsive screened Coulomb potential and is assigned a value in the range 0.1–0.15. Setting $\mu^* = 0.13$ and $T_c \sim 0.84$ K, the $\lambda_{ep}$ is calculated to be 0.453. On the other hand, $\lambda_{ep}$ can be extracted from the specific-heat measurement. From the inset of Fig. 3, we can see that the normalized specific-heat jump at $T_c$ is found to be $C_e/\gamma_n T_c = 1.54$. If the relation of $C_e/\gamma_n T_c = (1.43 + 0.942\lambda_{ep}^2 - 0.195\lambda_{ep}^3)$ is adopted, $\lambda_{ep}$ is estimated to be 0.365, close to the value of 0.453 extracted from the normal-state electrical resistivity. The small electron-phonon coupling is consistent with the BCS prediction for weak-coupling superconductivity. Furthermore, the small normal-state electronic coefficient $\gamma_n = 1.355$ mJ/mol K$^2$ determined from the specific-heat measurement indicates that WP has a relatively low density of states, in agreement with the earlier theoretical results [26], which accounts for the low transition temperature with $T_c \sim 0.8$ K.

In order to understand the superconductivity observed in WP, it is necessary to compare the interatomic distances between the nearest cations and the orbital overlap in the MnP-type (B31) structure including CrAs, CrP, and WP. As illustrated in Fig. 5, the transitional metal atom has three nearest-neighbor metal atoms. Apparently, the largest interatomic distance is the $b$-axis length, which determines the physical properties of the MnP-type compounds. Goodenough successfully explained the magnetic properties of the MnP-type (B31) structure by introducing the crystal-field and ligand field theory [27,28]. At ambient pressure, CrAs has a relatively large $b$-axis length of $b = 3.445$ Å that leads to a small $3d$-orbital overlap between $d_{x^2-y^2}$ bands, therefore, the $3d$ electrons are localized which accounts for the magnetic ordering in CrAs. However, as the $b$-axis length decreases to a critical value $b_c = 3.37$ Å under a pressure of $P = 1.0$ GPa [5], the larger orbital overlap between $3d_{x^2-y^2}$ makes CrAs adopt a collective state of the electrons without magnetic ordering and superconductivity emerges. As $P$ increases to 5.0 GPa, $b$ is further reduced and the superconductivity disappears. The $b$-axis length of CrP is only 3.11 Å [29], which is equivalent to that of CrAs under $P = 15.0$ GPa [30], and no superconductivity was observed. This indicates that the variation of the $b$-axis length plays an important role in determining the physical properties of MnP-type compounds. Compared to the pressure-driven superconducting CrAs and normal metal CrP, the intermediate $b$-axis length of $b = 3.25$ Å in WP, as shown in Fig. 5, suggests that superconductivity may emerge. On the other hand, according to Matthias rule [31], the superconductivity prefers to emerge at a peak density of states (DOS) at the Fermi level. However, CrP has a diplike DOS [6,30],

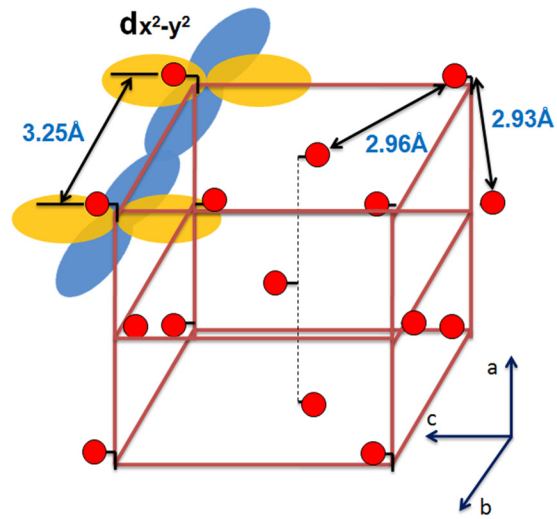


FIG. 5. Cation sublattice of unit cell of WP with the indicated distances between the tungsten atoms. The components of $d_{x^2-y^2}$ along the $b$ and $c$ axis are represented by the blue and yellow lobes, respectively.

which contradicts the Matthias rule. Additionally, CrP is far away from spin fluctuation dome. Combining the above two facts, it can be understood why CrP is not a superconductor. Compared to Pauli paramagnetism observed in CrP [5], WP exhibits diamagnetism in a broad range near room temperature [10]; this implies that the band-structure effect decreases the effective mass $m^*$ and Landau diamagnetism dominates the magnetic susceptibility. In comparison with $3d$ electrons in CrAs, $5d$ electrons in WP have an extended wave function and larger orbital overlap indicated by the blue lobes; this may be associated with the superconductivity observed in WP.

Very recently, WP was predicted to be a topological high-symmetry line semimetal when spin-orbit coupling (SOC) was considered [32]. So more experiments need to be carried out to establish the relationship of superconductivity and topological structure in WP.

## IV. CONCLUSIONS

In summary, high-quality WP single crystals were successfully prepared by chemical vapor transport method. Combining the electrical resistivity, ac magnetic susceptibility, and specific-heat measurements, we demonstrated that WP is an intrinsic superconductor with $T_c \sim 0.8$ K in MnP-type family at ambient pressure. Additionally, WP is a superconductor in $5d$-transition metal phosphides. Therefore, our study offers a platform to study the superconducting mechanism and may shed light to search for new superconductors in MnP-type compounds.

## ACKNOWLEDGMENTS

This work was supported by the National Basic Research Program of China (Grants No. 2016YFA0300600, No. 2017YFA0302901, No. 2015CB921101, and No. 2015CB921300), the National Natural Science Foundation of China (Grants No. 11874406, No. 11674375, and No. 11634015), and the Strategic Priority Research Program of the Chinese Academy of Sciences (Grants No. XDB07020200, No. XDB25000000, and No. QYZDB-SSW-SLH013).

Z.Y.L. and W.W. contributed equally to this work.

[1] W. Wu, J.-G. Cheng, K. Matsubayashi, P. Kong, F. Lin, C. Jin, N. Wang, Y. Uwatoko, and J. Luo, Nat. Commun. **5**, 5508 (2014).
[2] H. Kotegawa, S. Nakahara, H. Tou, and H. Sugawara, J. Phys. Soc. Jpn. **83**, 093702 (2014).
[3] H. Kotegawa, S. Nakahara, R. Akamatsu, H. Tou, H. Sugawara, and H. Harima, Phys. Rev. Lett. **114**, 117002 (2015).
[4] J.-G. Cheng, K. Matsubayashi, W. Wu, J. P. Sun, F. K. Lin, J. L. Luo, and Y. Uwatoko, Phys. Rev. Lett. **114**, 117001 (2015).
[5] K. Motizuki, H. Ido, T. Itoh, and M. Morifuji, *Electronic Structure and Magnetism of 3d-Transition Metal Pnictides*, Springer Series in Materials Science (Springer-Verlag, Berlin, 2010).
[6] W. Tremel, R. Hoffmann, and J. Silvestre, J. Am. Chem. Soc. **108**, 5174 (1986).
[7] C. C. Becerra, N. F. Oliveira, and A. C. Migliano, J. Appl. Phys. **63**, 3092 (1988).
[8] B. Westerstrandh, L. Lundgren, U. Gäfvertl, and B. Carlssona, Phys. Scr. **15**, 276 (1977).
[9] T. Nozue, H. Kobayashi, H. Yamagami, T. Suzuki, and T. Kamimura, J. Magn. Soc. Jpn. **23**, 430 (1999).
[10] We measured electrical resistivity and dc magnetic susceptibility of single crystals of CoP and WP.
[11] D. Hirai, T. Takayama, D. Hashizume, and H. Takagi, Phys. Rev. B **85**, 140509(R) (2012).
[12] B. W. Roberts, *Superconductive Materials and Some of Their Properties* (National Bureau of Standards, Washington, DC, 1969).
[13] J. G. Bednorz and K. A. Müller, Z. Phys. B **64**, 189 (1986).
[14] Y. Kamihara, T. Watanabe, M. Hirano, and H. Hosono, J. Am. Chem. Soc. **130**, 3296 (2008).
[15] L. B. McCusker, R. B. Von Dreele, D. E. Cox, D. Louër, and P. Scardi, J. Appl. Crystallogr. **32**, 36 (1999).
[16] S. Rundqvist and T. Lundström, Acta. Chem. Scand. **17**, 37 (1963).
[17] J. Martin and R. Gruehn, Solid State Ionics **43**, 19 (1990).
[18] R. Guérin, M. Sergent, and J. Prigent, Mat. Res. Bull. **10**, 957 (1975).
[19] S. Motojima and T. Higashi, J. Cryst. Growth. **71**, 639 (1985).
[20] L. X. Yang, Z. K. Liu, Y. Sun, H. Peng, H. F. Yang, T. Zhang, B. Zhou, Y. Zhang, Y. F. Guo, M. Rahn, D. Prabhakaran, Z. Hussain, S.-K. Mo, C. Felser, B. Yan, and Y. L. Chen, Nat. Phys. **11**, 728 (2015).
[21] Z. K. Liu, L. X. Yang, Y. Sun, T. Zhang, H. Peng, H. F. Yang, C. Chen, Y. Zhang, Y. F. Guo, D. Prabhakaran, M. Schmidt, Z. Hussain, S.-K. Mo, C. Felser, B. Yan, and Y. L. Chen, Nat. Mater. **15**, 27 (2016).
[22] G. R. Stewart, Rev. Mod. Phys. **83**, 1589 (2011).
[23] X. Zhu, B. Lv, F. Wei, Y. Xue, B. Lorenz, L. Deng, Y. Sun, and C.-W. Chu, Phys. Rev. B **87**, 024508 (2013).
[24] M. S. Fuhrer, Physics **3**, 106 (2010).
[25] W. L. McMillan, Phys. Rev. **167**, 331 (1968).
[26] G. Jaiganesh, R. D. Eithiraj, and G. Kalpana, Comput. Mater. Sci. **49**, 112 (2010).
[27] J. B. Goodenough, *Magnetism and the Chemical Bond* (Interscience/Wiley, New York, 1963).
[28] N. Menyuk, J. A. Kafalas, K. Dwight, and J. B. Goodenough, Phys. Rev. **177**, 942 (1969).
[29] K. Kanaya, S. Abe, H. Yoshida, K. Kamigaki, and T. Kaneko, J. Alloys. Compd. **383**, 189 (2004).
[30] Q. Niu, W. C. Yu, K. Y. Yip, Z. L. Lim, H. Kotegawa, E. Matsuoka, H. Sugawara, H. Tou, Y. Yanase, and Swee K. Goh, Nat. Commun. **8**, 15358 (2017).
[31] T. H. Geballe and J. K. Hulm, *Bernd Theodor Matthias* (National Academies Press, Washington, DC, 1996).
[32] T. T. Zhang, Y. Jiang, Z. D. Song, H. Huang, Y. Q. He, Z. Fang, H. M. Weng, and C. Fang, Nature (London) **566**, 475 (2019).